Journal of Materials Chemistry A

Accepted Manuscript

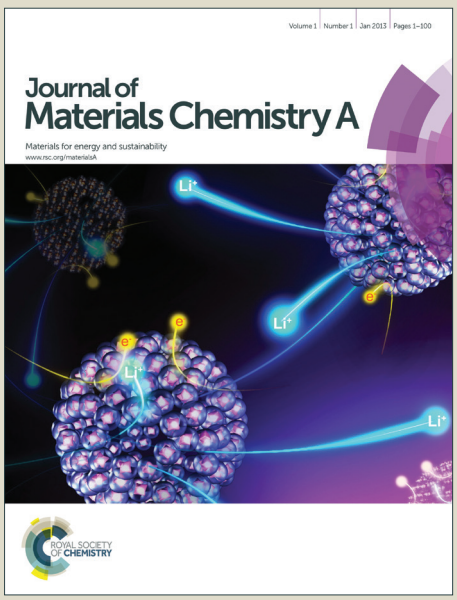

ROYAL SOCIETY OF CHEMISTRY

www.rsc.org/materialsA

Table of Content

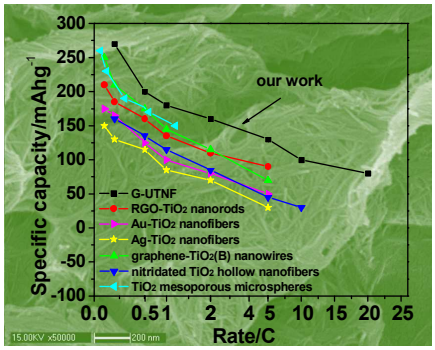

Graphene supported ultralong TiO_2 nanofibers from the commercial titania is synthesized with enhanced electrochemical performances.

Facile Synthesis of Graphene Supported Ultralong TiO_2 Nanofibers from the Commercial Titania for High Performance Lithium-Ion Batteries

Guifang Gu [a], Jianli Cheng [a,b,], Xiaodong Li [a], Wei Ni [a], Qun Guan [a], Guoxing Qu [a], Bin Wang [a *]*

[a] *Institute of Chemical Materials, China Academy of Engineering Physics, Mianyang 621900, Sichuan, P.R. China.*

[b] *State Key Laboratory of Molecular Engineering of Polymers (Fudan University)*

*Address correspondence to binwang@caep.cn; edward.bwang@gmail.com; Fax: (+86)816-2544 426.

Abstract

Novel nanocomposites consisted of two-dimensional graphene nanosheets and ultralong TiO_2 nanofibers are fabricated via a simple one-pot hydrothermal reaction using commercial TiO_2 particles as inorganic precursors. Complex chemical synthesis processes and high cost precursors can be avoided. When used as anodes of lithium ion batteries, the obtained nanocomposites exhibit a superior rate capability and an excellent long-term cycling stability. The nanocomposites maintain a charge capacity of 85 mA h g^{-1} at 20 C, while the TiO_2 nanofibers fail when cycled at 5 C. The nanocomposites also demonstrate an excellent cycling stability with a charge capacity of 92 mA h g^{-1} after 1000 cycles at 10 C, approximately three-fold capacity of the TiO_2 nanofibers. The superior electrochemical performance can be attributed to the hybrid structure of the graphene nanosheets and the ultralong TiO_2 nanofibers. The graphene nanosheets provide high electronic conductive pathways and work as protected layers to keep the active material integrating during charging/discharging processes. The ultralong TiO_2 nanofibers with high specific surface area have a short ion diffusion distance and provide more accessible sites. By combining the advantages of the graphene nansheets and TiO_2 nanofibers, the nanocomposites possess obviously improved electrochemical performances.

Introduction

There has been particular interest in anatase TiO_2 as an alternative anode material for high power lithium ion batteries (LIBs) due to its high electrochemical potential, structural stability, low price, abundance and safety.[1-4] Its high potential of higher than 1.7 V versus Li^+/Li is inherently safe because of avoiding the lithium plating on the negative electrode and thus enabling to charge-discharge at extremely high rates. Furthermore, the low volume expansion during lithium intercalation/deintercalation (3−4%) can greatly benefit the stability of long cycle life.[5, 6] However, the poor conductivity of TiO_2-based anodes limits their rate capability.[7-9] One effective approach to improve the ionic and electronic conductivity of the TiO_2 material is to blend nanostructured TiO_2 with highly conductive materials. Recently, hybrid TiO_2-based nanocomposites, such as TiO_2-CNT,[8, 10, 11] TiO_2-RuO_2,[12] TiO_2-Ni,[13] and TiO_2-graphene,[14-16] have been synthesized and tested in LIBs.

Among the conductive materials, two-dimensional graphene nanosheets, possessing high electronic conductivity, high specific surface area, and excellent mechanical properties, are very attractive as conductive substrates. By carefully controlling the synthesis condition, TiO_2 nanoparticles,[17-19] TiO2 nanobundles,[20] TiO_2 nanospheres,[21, 22] TiO_2 nanocrystals[14, 23] and TiO_2 nanorods[24-26] on graphene nanosheets have been reported. The obtained TiO_2-graphene nanocomposites can provide a high rate capability and a long cycling life. For the synthesis of TiO_2-graphene nanocomposites, organic precursors such as titanium isopropoxide[27-29], tetrabutyl titanate[20, 26] and titanium tetrabutoxide[8, 14] are used. However, these organic precursors

are expensive and sensitive to water. Meanwhile, to help the nucleation of TiO_2 on graphene oxides, the hydrolysis speed of organic precursors should be controlled by controlling the pH of the solution or using organic solvent. However, the complexity of the synthesis condition and the high cost of the precursors make the obtained TiO_2-graphene nanocomposites less desirable as electrode materials. Meanwhile, one dimensional nanofibers among different morphologies of TiO_2 have attracted particular interest to LIBs owing to large specific surface area, fast ion and electron transport pathways, and good accommodation to the volume change during the cycling processes.[5,30-32] However, to the best of our knowledge, there is no report about the graphene nanosheets supported anatase TiO_2 nanofibers nanocomposites as anodes of LIBs.

Herein, we report a facile synthetic route to obtain the nanocomposites consisting of ultralong anatase TiO_2 nanofibers and graphene, which the ultralong TiO_2 nanofibers are anchored on graphene nanosheets by a one-pot hydrothermal reaction by using commercial TiO_2 particles as inorganic precursors and commercial graphene oxide as substrates. The obtained graphene nanosheets supported ultralong TiO_2 nanofibers nanocomposites exhibit a superior rate capability, with the capacity of 128 mA h g^{-1} at 5 C, 104 mA h g^{-1} at 10 C, and 85 mA h g^{-1} at 20 C, respectively. More importantly, a stable capacity of 220 mA h g^{-1} can be delivered when the rate is reduced back to 0.2 C, suggesting the good structural stability of the nanocomposites.

Experimental

Synthesis of graphene nanosheets supported ultralong TiO_2 nanofibers nanocomposites (G- UTNF)

A mixture of TiO_2 powder (0.4 g, rutile, Aldrich) and 20 ml graphene oxide (GO) solution (5 mg/mL, Sinocarbon Materials Technology Co., Ltd., China) was added into NaOH (20 mL, 10 M) and then sonicated in an ultrasonic bath for 30 min. The solution was transferred into a Teflon-lined stainless autoclave which was heated to 150 ^oC and maintained for 40 h to make TiO_2 transform to $Na_2Ti_3O_7$. After cooling, the precipitations were collected and washed with distilled water and HCl solution (0.05 M). This ion exchange process can make the composite of GO and $Na_2Ti_3O_7$ (GO-$Na_2Ti_3O_7$) transform to the composite of GO and $H_2Ti_3O_7$ (GO- $H_2Ti_3O_7$). After drying at 70 ^oC for 12 h, the resulting powders were heat treated at 500 ^oC for 4 h in a N_2-flowing tube furnace. The final product was named as G- UTNF.

For the TiO_2 nanofibers, TiO_2 powder (0.4 g, rutile, Aldrich) was used as a raw material instead of a mixture of TiO_2 powder and graphene oxide, and hydrothermal temperature was maintained at 150 ^oC for 40 h. The final product named as TiO_2 nanofibers can be obtained by the heat treatment of $H_2Ti_3O_7$ precursor at 500 ^oC for 4 h in air.

Materials Characterization

X-ray diffraction (XRD) patterns were acquired using bruker AXS D8 ADVANCE with monochromatized Cu Kα radiation. The morphologies were characterized using field emission scanning electron microscopy (FESEM, Carl Zeiss SMT Pte Ltd., Ultra 55) and high resolution transmission electron microscopy (HR-TEM, JEOL 2100F). The thermogravimetric analysis (TGA, METTLER TOLEDO ATAR^e System, TGA 1) was carried out at a heating rate of 20 ^oC min^{-1} from room temperature to 700 ^oC under

airflow. The pore size distributions were calculated from the desorption branch of the N_2 adsorption/desorption isotherm curves using a multi-point Brunauer-Emmett-Teller surface area analyzer (BET, Beijing JWGB Sci&Tech Co., Ltd., JW-BK300). Raman spectroscopy was recorded from 100 to 2000 cm^{-1} on a Renishaw Invia Raman microscope excited by an argon ion laser beam (514.5 nm, 20 mW).

Electrochemical Measurements

The working electrode was prepared by mixing the as-prepared active component with acetylene black and polyvinylidene difluoride (PVDF) at a weight ratio of 8:1:1. The resultant slurry was then uniformly casted on a Cu foil current collector and dried overnight under vacuum. The loading of the electrode is about ~2 mg cm^{-2}. CR2032-type coin cells were assembled in a glove box for electrochemical characterization. The electrolyte was 1 M $LiPF_6$ in a mixture of ethylene carbonate and dimethyl carbonate (1:2). Li metal foils were used as the counter and reference electrodes. The electrochemical performances of the electrodes were characterized by an LANHE battery testing system at room temperature. The cells were galvanostatically charged and discharged at different current densities within the range of 1.0-3.0 V. The specific capacity was calculated by the TiO_2 mass of the composite material.

Results and discussion

Nanostructured TiO_2 with various morphologies like nanosheets, nanorods, and nanowires has been reported by hydrothermal treatment of TiO_2 particles in strong alkaline solution.[33-36] It has been reported that the TiO_2 particles can dissolve in strong alkaline solution and recrystallize into different morphologies during the hydrothermal

treatment.[37] In this work, the modified hydrothermal method is used to synthesize the graphene nanosheets supported ultralong TiO_2 nanofibers nanocomposites (G- UTNF), in which commercial TiO_2 particles and GO are treated with concentrated NaOH solution. During the hydrothermal processes, the GO nanosheets acted as nucleation sites for the recrystallization of Ti-containing complex. The fabrication processes of TiO_2 nanofibers and G- UTNF nanocomposites are illustrated in Fig. 1.

Fig. 2 shows the SEM images of the G- UTNF, the TiO_2 nanofibers and their precursors. It can be seen from the Fig. 2a and b that the GO- $H_2Ti_3O_7$ precursor consists of numerous $H_2Ti_3O_7$ nanofibers anchoring on the GO nanosheets with the length of several hundred nanometers. After heat-treatment, it can be seen from Fig. 2c and d that the G- UTNF keeps well the morphologies of the precursor, which long TiO_2 nanofibers are uniformly dispersed on graphene nanosheets. It indicates that the GO can not only promote the nucleation and growth of Ti-containing complex, but also work as good substrates to retain the nanofiber structure during the calcination. In contrast, without the support of graphene nanosheets, the $H_2Ti_3O_7$ precursor is composed of relatively short nanofibers with the length of 200-500nm (Fig. 2e and 2f). After heat-treatment, the $H_2Ti_3O_7$ changes to TiO_2 nanofiber with similar length (Fig. 2g and h).

TEM images of the G- UTNF (Fig. 3a and b) show that numerous TiO_2 nanofibers with length of several hundred nanometers are uniformly dispersed on the graphene nanosheets. HR-TEM image in Fig. 3c shows that the TiO_2 nanofibers with width of approximately 8 nm are well crystallized and the interplanar distance between adjacent lattice planes is about 0.35 nm, which corresponds to the (101) plane of anatase TiO_2.

The fast Fourier transform (FFT) image indicates well crystallized and long-range crystalline order of the TiO_2 nanofibers (Fig. 3d).[37]

XRD patterns of the as-prepared G- UTNF nanocomposites and its GO- $H_2Ti_3O_7$ precursor are shown in Fig. 4a. Commercial TiO_2 particles transform to $H_2Ti_3O_7$ nanofibers on the surface of GO after the hydrothermal reaction and the followed acid wash processes, which are in good agreement with the reported results.[37] By the following heat treating, the GO- $H_2Ti_3O_7$ changes to G- UTNF due to the transformation of GO and $H_2Ti_3O_7$ at high temperature. Simultaneously, the GO is reduced to graphene according to the disappearance of diffraction peak of GO at approximately 10° in the GO- $H_2Ti_3O_7$. The diffraction pattern of the G- UTNF is in good agreement with that of anatase TiO_2 (JCPDS No. 21-1272). The diffraction peak of the graphene is somewhat overlapped with the (101) plane of TiO_2. The XRD patterns of the TiO_2 nanofibers and the $H_2Ti_3O_7$ precursor can be seen in Fig. S1 in Supporting Information. The thermogravimetric analysis (TGA) is performed to determine the content of graphene in the G- UTNF as shown in Fig. S2. The content of graphene in the G- UTNF is about 13.5%.

Thermal treatment of the GO nanosheets can remove a portion of functional groups on their basal planes, which results in the recovery of the electronic properties of the graphene nanosheets. To better know the reduction processes, the G- UTNF, TiO_2 nanofibers and bare GO are monitored by the Raman spectroscopy (Fig. 4b). Five typical peaks of anatase TiO_2 at 149, 199, 397, 513 and 639 cm^{-1} are observed for the G- UTNF and TiO_2 nanofibers. While two characteristic bands of carbon at 1372 cm^{-1}

(D band) and at 1598 cm^{-1} (G band) are observed for the G- UTNF and bare GO. The D band is related to edges, defects and disordered carbon atoms, whereas the G band is ascribed to the zone centre E_{2g} mode, corresponding to the ordered sp^2-bonded carbon atoms.[15, 38] The change of intensity ratio of the D band to the G band, I_D/I_G, is used to monitor the structural change of the graphene nanosheets.[39, 40] The I_D/I_G of bare GO is 1.34, while the I_D/I_G of G- UTNF is 1.21 in Fig. 4b. The decrease of the I_D/I_G ratio for G- UTNF indicates that the defects are reduced after the removal of the functional groups on the GO during thermal treatment, which suggests that the GO in the nanocomposites has reverted to graphene.

The surface and pore properties of the nanocomposites are characterized by nitrogen adsorption/desorption measurements as shown in Fig. S3. The surface area is calculated by the multi-point Brunauer-Emmett-Teller (BET) method. The G- UTNF composites have a specific surface area of 185 $m^2 g^{-1}$, which is much higher than that of the TiO_2 nanofibers (125 $m^2 g^{-1}$). Large specific surface area can provide more active sites and more contact area for the electrolyte, which may benefit the electrolyte wetting and improve the electrochemical performances of the nanocomposite.[41, 42]

To better know the electrochemical properties of the nanocomposites, the G- UTNF and TiO_2 nanofibers are investigated as anode materials of LIBs. Fig. 5a and b show the cyclic voltammograms (CV) of the G- UTNF electrode and TiO_2 nanofibers electrode for the first six scans at a scan rate of 0.2 mV s^{-1}, respectively. It can be seen from Fig. 5a that the cathodic peak in the first scan is located at ~1.55 V vs. Li^+/Li, which corresponds to the reduction of Ti^{4+} to Ti^{3+} or the formation of an inactive solid

electrolyte interphase (SEI) on the surface of the active material.[43-45] In the subsequent cycles, the cathodic peak shifts to higher voltage (~1.7 V vs. Li^+/Li). Variation in the peak position is mainly due to the structural re-arrangement of TiO_2 crystal lattice.[44, 46] Consistent with the results of the previous studies, [47] two peaks at approximately 1.7 V (cathodic peak) and 2.1 V (anodic peak) are observed in the CV curves of both G-UTNF electrode and TiO_2 nanofibers electrode, which can be attributed to the lithium insertion/deinsertion processes into/from the anatase. For G- UTNF electrode, there is no obvious change of the peak position and intensity in the several cycles, indicating the good stability and high reversibility of the electrode processes ($TiO_2 + xLi^+ + xe^- \leftrightarrow Li_xTiO_2$ ($x \leqslant 1$), where x is the amount of inserted Li^+).[15, 47-49] However, the peak intensity of the TiO_2 nanofibers electrode declines with the cycling, indicated that some irreversible reactions occurred in the electrode. Furthermore, the gradually decreased peak at approximately 2.35 V are detected for G- UTNF electrode, which may be attributed to the trace of rutile TiO_2.[50] The existence of the trace of rutile TiO_2 in the nanocomposites is confirmed by TEM characterization (see Fig. S4). It might be caused by the phase transformation during the heat treatment which makes anatase transform to rutile.

Fig. 5c shows the galvanostatic charge-discharge profiles of the G- UTNF electrode and the TiO_2 nanofibers electrode in the first and fifth cycles. Two distinct voltage plateaus can be observed during the charge-discharge processes which are in agreement with the above CV results. The discharge curves can be divided into three stages: a fast potential drop starting from the open-circuit potential to ~1.7 V, the plateau

region at ~1.7 V and the following long voltage slope, which can be attributed to the solid-solution diffusion process, the insertion of Li^+ and the surface/interfacial Li^+ storage on the anatase, respectively. Furthermore, the plateau at approximately 2.35 V in the first CV scan of G- UTNF electrode also can be assigned to the trace of rutile TiO_2. The G- UTNF electrode exhibits an initial capacity of 459 mA h g^{-1}, which is much higher than that of TiO_2 nanofibers electrode (328 mA h g^{-1}). This improvement could be attributed to the integration of highly electronic conducting graphene nanosheets and the ultralong TiO_2 nanofibers.

Fig. 5d displays the rate capabilities of the G- UTNF electrode and TiO_2 nanofibers electrode at different rates from 0.2 C to 20 C. As expected, the G- UTNF electrode exhibits a superior rate capability compared to the TiO_2 nanofibers electrode at the same testing condition, with the capacity of 128 mA h g^{-1} at 5 C, 104 mA h g^{-1} at 10 C, and 85 mA h g^{-1} at 20 C. More importantly, a stable capacity of 220 mA h g^{-1} can be delivered when the rate is reduced back to 0.2 C, suggesting a good structural stability and high reversibility of the nanocomposites even after high rate charging-discharging tests. As a contrast, without the highly conductive graphene, the TiO_2 nanofibers electrode shows a very poor rate capability. With the rate increasing from 0.2 to 20 C, the specific capacity drops significantly. It even could not be charged/ discharged at high rate of 5 C. Fig. 5e shows the rate capability comparisons between the G- UTNF electrode and several recently reported TiO_2-based electrodes such as the RGO-TiO_2 nanorods,[24] Au-TiO_2 nanofibers,[30] Ag-TiO_2 nanofibers,[30] graphene-TiO_2(B) nanowires,[51] nitridated TiO_2 hollow nanofibers[4] and TiO_2 mesoporous microspheres.[52]

It can be seen that the rate capability of the G- UTNF electrode is superior to that of the reported literatures.[4, 24, 30, 51, 52]

To evaluate the long-term cycling ability at high rate, the G- UTNF electrode and the TiO_2 nanofibers electrode are tested at high rates of 5 C and 10 C over 1000 cycles. It can be seen clearly in Fig. S5 and Fig. 5f that the G- UTNF electrode demonstrates an excellent cycling stability with a charge capacity of 125 mA h g^{-1} at 5 C and 92 mA h g^{-1} at 10 C after 1000 cycles. The G- UTNF electrode keeps a capacity retention of 71% with nearly 99% Coulombic efficiency, approximately three-fold capacity of the TiO_2 nanofibers electrode, implying that the side reactions are effectively restricted in the graphene supported ultralong TiO_2 nanofibers nanocomposites.[53, 54]

The electrochemical impedance spectroscopy (EIS) is utilized to validate the influence of graphene on the electronic conductivity of TiO_2 nanofibers. The Nyquist plots after different cycles are shown in Fig. 6. The EIS plots comprise three frequency regions. The formation of contact resistance and/or SEI film happens at the high frequency region. The middle frequency region can be assigned to the charge-transfer (CT) resistance between the electrode/electrolyte interfaces. The low frequency region reflects the lithium diffusion kinetics which generate Warburg tail. From Fig. 6, it can be observed that the diameters of the semicircles in the middle-frequency region for G-UTNF (Fig. 6a) are remarkably smaller than those of the TiO_2 nanofibers (Fig. 6b), which show the decreased CT resistance in the G- UTNF. The decrease of CT resistance is mainly attributed to the enhanced electronic conductivity offered by graphene nanosheets, which results in faster diffusion kinetics in G- UTNF. There are two

dynamic competitive processes in the electrode, namely the activation processes of the electrode (such as the formation of the surface passivation film, the re-arrangement of the electrode and the wetting of the electrode by the electrolyte) and the degradation of the electrode (such as the slow pulverization of electrode surface and the destroy of surface film). For the G- UTNF, the CT resistance increases a little bit from 10^{th} cycle (11.3 Ω) to 20^{th} cycle (14.2 Ω), which may correspond to the gradual formation of surface passivation film on the new material in the initial processes and the corresponding electrode deformation and material interface activation, suggesting a slight degradation of charge transfer kinetics.[45, 55, 56] After that, the CT resistance keeps gradually decreasing, which may correspond to the formation of good conductive pathway in the composites and the re-arrangement of the electrode at 5C fast charge-discharge processes.[57, 58] However, detailed mechanism involved is not yet fully understood which should be further examined in the future work. On the contrary, it can be seen from Fig. 6b that, without the integration of graphene nanosheets, the CT resistance in the TiO_2 nanofibers is about 35 Ω after 20 cycles and increases to approximately 45 Ω after 200 cycles. This phenomena further prove the improvement in electronic conductivity in the nanocomposites, which are consistent with their rate capability performance.

As can be seen from the above results, the graphene nanosheets supported ultralong TiO_2 nanofibers nanocomposites possess excellent electrochemical properties in terms of high specific capacity, excellent rate-capability and stable cycling performance. These results can be attributed to the following reasons. First of all, the

graphene nanosheets significantly improve the entire electronic conductivity, which obviously enhance the electrochemical performance. Second, the interconnected TiO_2 nanofibers provide shorter electron transport lengths and larger electrode/electrolyte contact area, which can benefit the charge-transfer kinetics. Third, the uniformly dispersed TiO_2 nanofibers prevent the π-π restacking of interlayer graphene nanosheets, which can accommodate the strain generated in the lithium-ion insertion/deinsertion processes to maintain the structural stability of electrode material.

Conclusions

In summary, we have developed a facile scalable synthetic route for preparation of graphene nanosheets supported ultralong TiO_2 nanofibers nanocomposites as anode materials for LIBs. This method is based on hydrothermal treatment of commercial TiO_2 particles and GO suspension in concentrated NaOH solution. The as-prepared TiO_2-graphene nanocomposites exhibit a high lithium storage capacity and an excellent cycling performance. The nanocomposites can maintain an excellent high-rate long-term cycling stability with a high charge capacity of 92 mA h g^{-1} after 1000 cycles at 10 C. The synergistic effects of the nanosized TiO_2 fibers, high electronic conductivity pathways provided by graphene nanosheets and mesoporous structure lead to superior electrochemical performance.

Acknowledgements

This work is supported by the Startup Foundation of China Academy of Engineering Physics, Institute of Chemical Materials (KJCX201301 and KJCX201306), National Natural Science Foundation of China (No. 21401177), the "1000plan" from the Chinese

Government, the R&D Foundation of China Academy of Engineering Physics (2014B0302036), and the Open Foundation of State Key Laboratory of Molecular Engineering of Polymers, Fudan University(K2013-19).

Electronic Supplementary Information Available

XRD patterns of the pristine TiO_2 nanofibers and its precursor. TGA curve of the G-TiO_2-N_2. Surface and pore properties of the G-TiO_2-N_2 and pristine TiO_2 nanofibers. HR-TEM image of the G-TiO_2-N_2. See DOI:10.1039/b000000x/

Notes and references:

1. B. Wang, H. Xin, X. Li, J. Cheng, G. Yang and F. Nie, *Sci. Rep-Uk*, 2014, **4**, 3729.
2. Y. Ren, Z. Liu, F. Pourpoint, A. R. Armstrong, C. P. Grey and P. G. Bruce, *Angew. Chem.*, 2012, **51**, 2206-2209.
3. L. Ji, Z. Lin, M. Alcoutlabi and X. Zhang, *Energy Environ.Sci.*, 2011, **4**, 2682-2699.
4. H. Han, T. Song, J.-Y. Bae, L. F. Nazar, H. Kim and U. Paik, *Energy Environ. Sci.*, 2011, **4**, 4532-4536.
5. X. Zhang, P. Suresh Kumar, V. Aravindan, H. H. Liu, J. Sundaramurthy, S. G. Mhaisalkar, H. M. Duong, S. Ramakrishna and S. Madhavi, *J. Phys. Chem. C*, 2012, **116**, 14780-14788.
6. D. Deng, M. G. Kim, J. Y. Lee and J. Cho, *Energy Environ.Sci.*, 2009, **2**, 818-837.
7. H. Han, T. Song, E.-K. Lee, A. Devadoss, Y. Jeon, J. Ha, Y.-C. Chung, Y.-M. Choi, Y.-G. Jung and U. Paik, *ACS nano*, 2012, **6**, 8308-8315.
8. I. Moriguchi, R. Hidaka, H. Yamada, T. Kudo, H. Murakami and N. Nakashima, *Adv. Mater.*, 2006, **18**, 69-73.
9. B. Wang, J. Cheng and Y. Wu, *J. Alloys Compd.*, 2012, **527**, 132-136.
10. F.-F. Cao, Y.-G. Guo, S.-F. Zheng, X.-L. Wu, L.-Y. Jiang, R.-R. Bi, L.-J. Wan and J. Maier, *Chem. Mater.*, 2010, **22**, 1908-1914.
11. S. L. Chen Lin, Nie Ping, Su Xiaofei, Zhang Xiaogang, Li Hongsen, *Acta Chim. Sin.*, 2012, **70**, 15-20.
12. Y. G. Guo, Y. S. Hu, W. Sigle and J. Maier, *Adv. Mater.*, 2007, **19**, 2087-2091.
13. W. Wang, M. Tian, A. Abdulagatov, S. M. George, Y. C. Lee and R. Yang, *Nano Lett.*, 2012, **12**, 655-660.
14. L. Sun, Z. Zhao, Y. Zhou and L. Liu, *Nanoscale*, 2012, **4**, 613-620.
15. J. Shen, B. Yan, M. Shi, H. Ma, N. Li and M. Ye, *J. Mater. Chem.*, 2011, **21**, 3415-3421.
16. J. S. Chen, Z. Wang, X. C. Dong, P. Chen and X. W. Lou, *Nanoscale*, 2011, **3**, 2158-2161.
17. C. Zhu, S. Guo, P. Wang, L. Xing, Y. Fang, Y. Zhai and S. Dong, *Chem. Commun.*, 2010, **46**, 7148-7150.
18. J. S. Lee, K. H. You and C. B. Park, *Adv. Mater.*, 2012, **24**, 1084-1088.
19. D. Wang, D. Choi, J. Li, Z. Yang, Z. Nie, R. Kou, D. Hu, C. Wang, L. V. Saraf, J. Zhang, I. A. Aksay and J. Liu, *ACS Nano*, 2009, **3**, 907-914.
20. M. Zhen, X. Guo, G. Gao, Z. Zhou and L. Liu, *Chem. Commun.*, 2014, **50**, 11915-11918.
21. J. Lu, M. Wang, Y. Li and C. Deng, *Nanoscale*, 2012, **4**, 1577-1580.
22. N. Li, G. Liu, C. Zhen, F. Li, L. Zhang and H.-M. Cheng, *Adv. Funct. Mater.*, 2011, **21**, 1717-1722.

23. V. Štengl, D. Popelková and P. Vláčil, *J. Phys. Chem. C*, 2011, **115**, 25209-25218.
24. L. He, R. Ma, N. Du, J. Ren, T. Wong, Y. Li and S. T. Lee, *J. Mater. Chem.*, 2012, **22**, 19061-19066.
25. C. Wu, X. Huang, L. Xie, X. Wu, J. Yu and P. Jiang, *J. Mater. Chem.*, 2011, **21**, 17729-17736.
26. M. Zhen, S. Guo, G. Gao, Z. Zhou and L. Liu, *Chem. Commun.*, 2015, **51**, 507-510.
27. D. Eder and A. H. Windle, *Adv. Mater.*, 2008, **20**, 1787-1793.
28. J. S. Chen, H. Liu, S. Z. Qiao and X. W. Lou, *J. Mater. Chem.*, 2011, **21**, 5687-5692.
29. K. Saravanan, K. Ananthanarayanan and P. Balaya, *Energy Environ.Sci.*, 2010, **3**, 939-948.
30. S. H. Nam, H.-S. Shim, Y.-S. Kim, M. A. Dar, J. G. Kim and W. B. Kim, *ACS Appl. Mater. Interfaces*, 2010, **2**, 2046-2052.
31. M. V. Reddy, R. Jose, T. H. Teng, B. V. R. Chowdari and S. Ramakrishna, *Electrochim. Acta*, 2010, **55**, 3109-3117.
32. G. Sudant, E. Baudrin, D. Larcher and J.-M. Tarascon, *J. Mater. Chem.*, 2005, **15**, 1263-1269.
33. J. Cheng, B. Wang, H. L. Xin, C. Kim, F. Nie, X. Li, G. Yang and H. Huang, *J. Mater. Chem. A*, 2014, **2**, 2701-2707.
34. A. R. Armstrong, G. Armstrong, J. Canales and P. G. Bruce, *J. Power Sources*, 2005, **146**, 501-506.
35. S. Liu, H. Jia, L. Han, J. Wang, P. Gao, D. Xu, J. Yang and S. Che, *Adv. Mater.*, 2012, **24**, 3201-3204.
36. S.-J. Park, H. Kim, Y.-J. Kim and H. Lee, *Electrochim. Acta*, 2011, **56**, 5355-5362.
37. S.-T. Myung, N. Takahashi, S. Komaba, C. S. Yoon, Y.-K. Sun, K. Amine and H. Yashiro, *Adv. Funct. Mater.*, 2011, **21**, 3231-3241.
38. B. Wang, J. Cheng, Y. Wu, D. Wang and D. He, *J. Mater. Chem. A*, 2013, **1**, 1368-1373.
39. J. Cheng, H. Xin, H. Zheng and B. Wang, *J. Power Sources*, 2013, **232**, 152-158.
40. G. Zhou, D.-W. Wang, L.-C. Yin, N. Li, F. Li and H.-M. Cheng, *Acs Nano*, 2012, **6**, 3214-3223.
41. Q. Qu, Y. Zhu, X. Gao and Y. Wu, *Adv. Energy Mater.*, 2012, **2**, 950-955.
42. C. Liu, F. Li, L.-P. Ma and H.-M. Cheng, *Adv. Mater.*, 2010, **22**, E28-E62.
43. Z. Yang, G. Du, Q. Meng, Z. Guo, X. Yu, Z. Chen, T. Guo and R. Zeng, *J. Mater. Chem.*, 2012, **22**, 5848.
44. X. Zhang, V. Aravindan, P. S. Kumar, H. Liu, J. Sundaramurthy, S. Ramakrishna and S. Madhavi, *Nanoscale*, 2013, **5**, 5973.
45. R. Wang, C. Xu, J. Sun, Y. Liu, L. Gao and C. Lin, *Nanoscale*, 2013, **5**, 6960-6967.
46. V. Aravindan, W. Chuiling and S. Madhavi, *J. Mater. Chem.*, 2012, **22**, 16026-16031.
47. S. Ding, J. S. Chen, D. Luan, F. Y. Boey, S. Madhavi and X. W. Lou, *Chem. Commun.*, 2011, **47**, 5780-5782.
48. M. Wagemaker, W. J. H. Borghols and F. M. Mulder, *J. Am. Chem. Soc.*, 2007, **129**, 4323-4327.
49. J.-Y. Shin, D. Samuelis and J. Maier, *Adv. Funct. Mater.*, 2011, **21**, 3464-3472.
50. J. Shen, H. Wang, Y. Zhou, N. Ye, G. Li and L. Wang, *RSC Adv.*, 2012, **2**, 9173-9178.
51. J. Hou, R. Wu, P. Zhao, A. Chang, G. Ji, B. Gao and Q. Zhao, *Mater. Lett.*, 2013, **100**, 173-176.
52. J. Wang, Y. Zhou, Y. Hu, R. O'Hayre and Z. Shao, *J. Phys. Chem. C*, 2011, **115**, 2529-2536.
53. J. S. Chen, Y. L. Tan, C. M. Li, Y. L. Cheah, D. Luan, S. Madhavi, F. Y. C. Boey, L. A. Archer and X. W. Lou, *J. Am. Chem. Soc.*, 2010, **132**, 6124-6130.
54. J. B. Goodenough and Y. Kim, *Chem. Mater.*, 2010, **22**, 587-603.
55. M. Zhen, L. Su, Z. Yuan, L. Liu and Z. Zhou, RSC Adv., 2013, 3, 13696.
56. L. Su, Z. Zhou and M. Ren, Chem. Commun., 2010, 46, 2590-2592..
57. S.-q. Guo, X. Zhang, Z. Zhou, G.-d. Gao and L. Liu, J. Mater. Chem. A, 2014, 2, 9236.

58. J. Y. Choi, D. J. Lee, Y. M. Lee, Y. G. Lee, K. M. Kim, J. K. Park and K. Y. Cho, Adv. Funct. Mater., 2013, 23, 2108-2114.

Figure Caption:

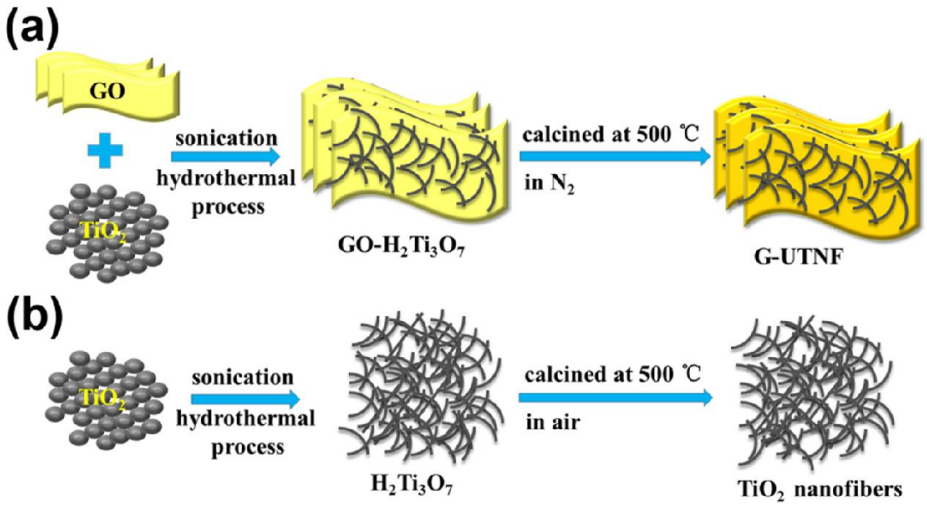

Fig. 1. Schematic illustration of synthesis processes of (a) graphene supported ultralong TiO_2 nanofibers nanocomposites (G- UTNF) and (b) TiO_2 nanofibers

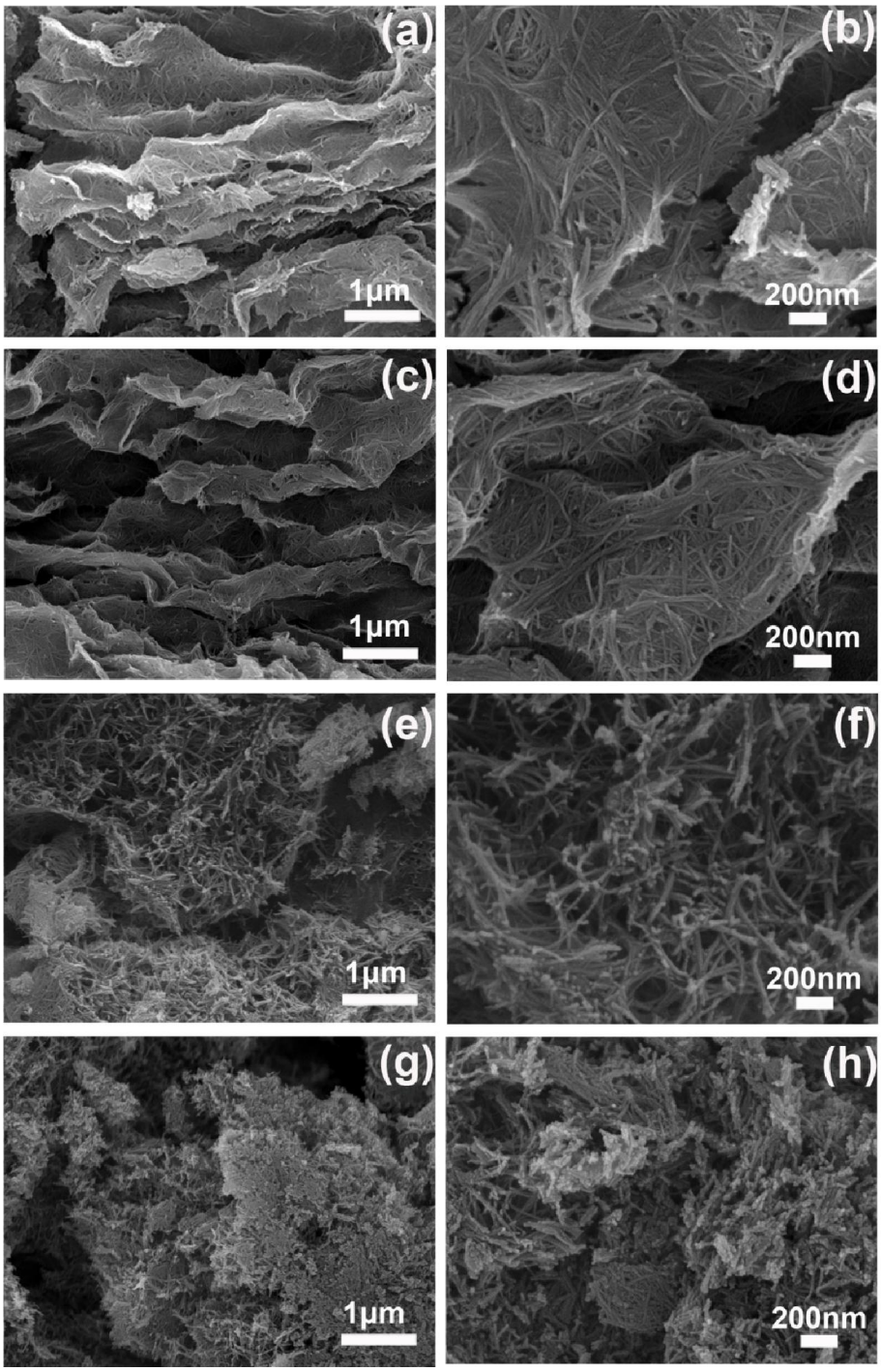

Fig. 2. SEM images of (a, b) the GO- $H_2Ti_3O_7$ precursor, (c, d) the G- UTNF, (e, f) the $H_2Ti_3O_7$ precursor and (g, h) the TiO_2 nanofibers.

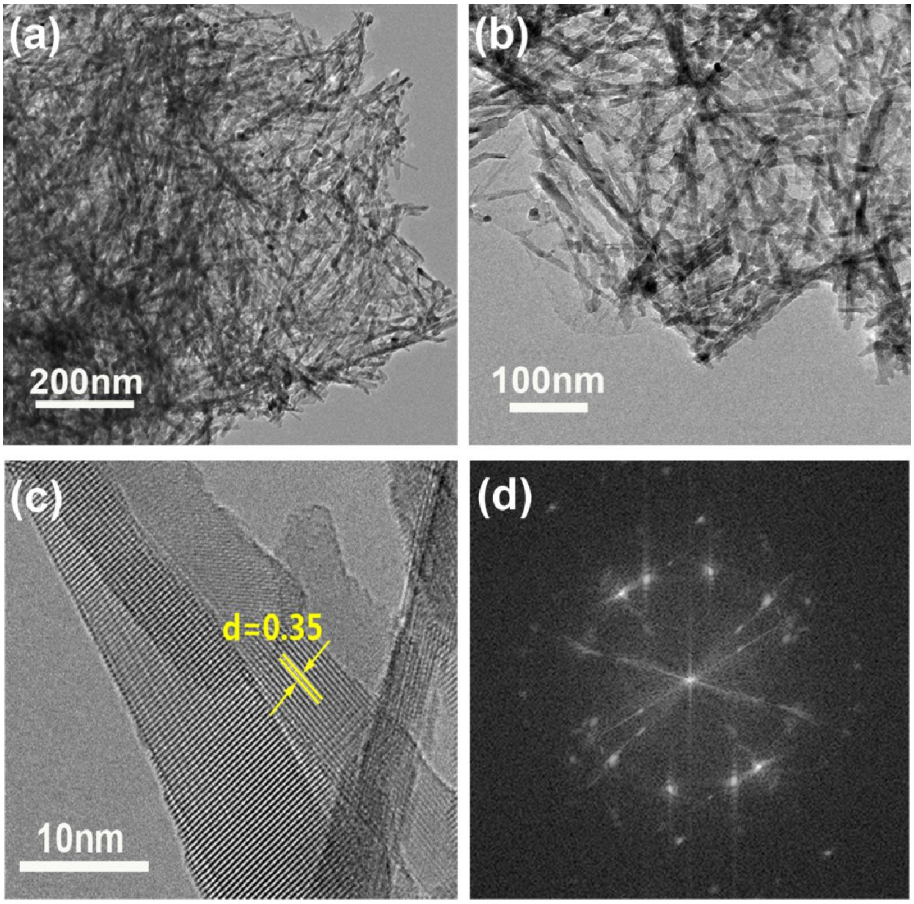

Fig. 3. (a, b) TEM images at different magnifications and (c) the HR-TEM image of the G- UTNF composites and (d) the corresponding FFT image.

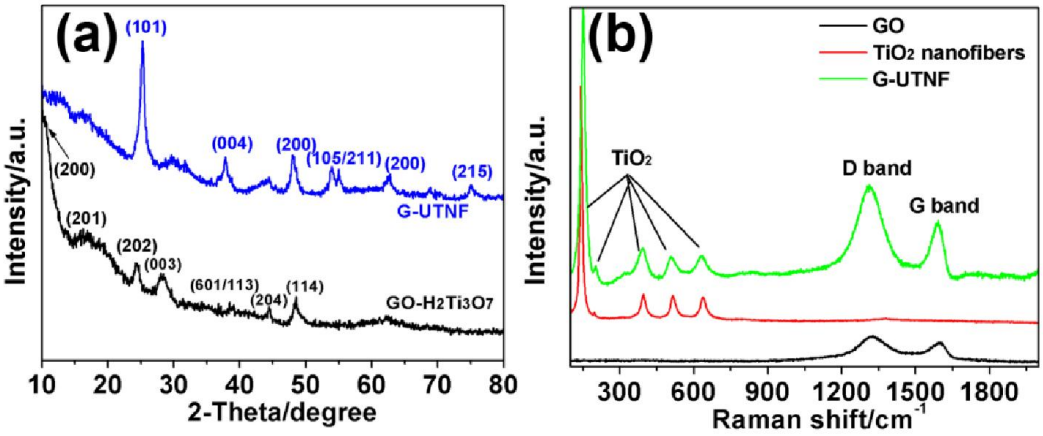

Fig. 4. (a) XRD patterns of the G- UTNF and its GO- $H_2Ti_3O_7$ precursor. (b) Raman spectra of the G- UTNF, the TiO_2 nanofibers and GO.

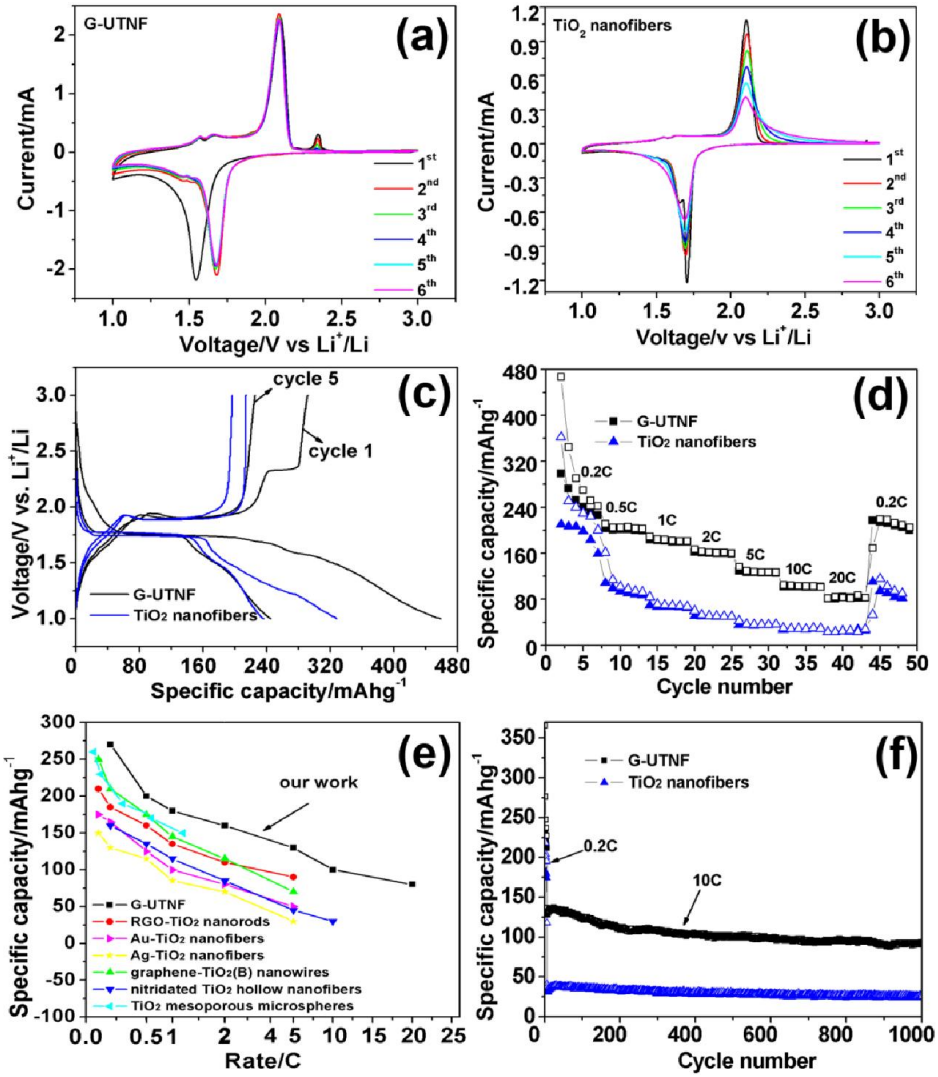

Fig. 5. Electrochemical measuremets. Cyclic voltammograms of the (a) G- UTNF composites and (b) TiO_2 nanofibers electrode at a scan rate of 0.2 mV s^{-1}; (c)The charge-discharge voltage profiles of the G- UTNF composites and TiO_2 nanofibers electrode in the first and fifth cycles, (d) the rate capability of the G- UTNF composites and TiO_2 nanofibers at different rates (e) the cycling performances of the G- UTNF composites and TiO_2 nanofibers at 10 C; (f) the comparisons of the G- UTNF with the reported results of TiO_2-based electrodes at different rates, RGO-TiO_2 nanorods,[24] Au-TiO_2 nanofibers,[30] Ag-TiO_2 nanofibers,[30] graphene-TiO_2(B) nanowires,[51] nitridated TiO_2 hollow nanofibers[4] and TiO_2 mesoporous microspheres.[52]

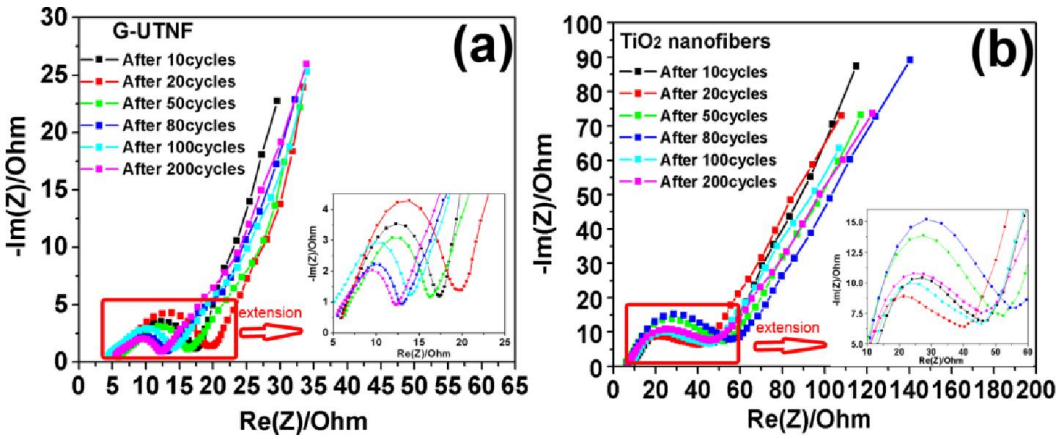

Fig. 6. Nyquist plots of (a) the G- UTNF composites electrode and (b) the TiO_2 nanofibers electrode at 5 C after different cycles.